Nanoscale

PAPER

View Article Online
View Journal | View Issue

Cite this: *Nanoscale*, 2014, **6**, 9846

Broadband antireflection and field emission properties of TiN-coated Si-nanopillars

Yuan-Ming Chang,*[a] Srikanth Ravipati,[b] Pin-Hsu Kao,[c] Jiann Shieh,[d] Fu-Hsiang Ko[b] and Jenh-Yih Juang*[a]

Received 7th April 2014
Accepted 13th June 2014

DOI: 10.1039/c4nr01874e

www.rsc.org/nanoscale

Broadband antireflection and field emission characteristics of silicon nanopillars (Si-NPs) fabricated by self-masking dry etching in hydrogen-containing plasma were systematically investigated. In particular, the effects of ultrathin (5–20 nm) titanium nitride (TiN) films deposited on Si-NPs by atomic layer deposition (ALD) on the optoelectronic properties were explored. The results showed that by coating the Si-NPs with a thin layer of TiN the antireflection capability of pristine Si-NPs can be significantly improved, especially in the wavelength range of 1000–1500 nm. The enhanced field emission characteristics of these TiN/Si-NP heterostructures suggest that, in addition to the reflectance suppression in the long wavelength range arising from the strong wavelength-dependent refractive index of TiN, the TiN-coating may have also significantly modified the effective work function at the TiN/Si interface as well.

Published on 17 June 2014. Downloaded by National Chiao Tung University on 25/12/2014 02:11:40.

Introduction

Over the last few decades, arrays of one-dimensional (1D) silicon nanostructures (Si-NSs) have attracted a tremendous amount of research attention due to their profound impacts in advancing the modern science and technologies.[1–3] Among the methods developed for fabricating the 1D-Si-NS, metallic nanoparticles, including gold, silver and nickel, have been playing an important role in serving as the bottom-up growth catalysts[4,5] or as metal-masks during the top-down galvanic displacement reaction[2] and dry etching processes.[6,7] Most of these techniques, however, require either complicated manufacturing processes and/or are time-consuming. Therefore, developing a simple fabrication scheme to create 1D-Si-NS in a controlled manner is of both fundamental and application significance. Very recently, we have demonstrated that self-assembled silver nano-dots (Ag-NDs) obtained from short time dc-sputtering could serve as a natural metal-mask in producing Si-NS with much improved anti-reflectivity in the wavelength range of 300–1000 nm.[8] Moreover, such Si-NS, when incorporated with a thin layer of ZnO derived from atomic layer deposition (ALD), could reduce the field emission turn-on field dramatically.[9] In the former case, the very low reflection loss obtained has been attributed to the establishment of a gradually decreasing refraction index gradient and reduction of diffraction loss by introducing the sub-wavelength spacing in the micron-sized 1D-Si-NS layer.[8] In the latter case, on the other hand, the inhibition of the forming native SiO_x layer and possible band-edge discontinuity resulting from the incorporation of an ultra-thin ALD-derived ZnO layer on Si-NSs are believed to play a prominent role.[9] A similar concept of introducing a chemically more stable surface coating to enhance the field emission properties of Si-NSs without altering their unique geometries has also been demonstrated in diamond-coated Si nanoemitters.[10,11] However, the antireflective properties of such coated-Si-NS heterostructures were not systematically explored.

Titanium nitride (TiN) is a midgap metal with a melting point of 2930 °C and a high thermal conductivity of ~19.2 W m^{-1} $°C^{-1}$, and is chemically inert under ambient conditions.[12] More interestingly, the work function of TiN has been reported to vary from 3.5–4.7 eV, depending on the preparation methods and templates used.[13–17] As a result, it has been extensively investigated and used as the gate electrode for effective work function control in various semiconductor field-effect semiconductor devices.[14–17] Moreover, its refractive index n is known to strongly depend on the illuminating wavelength (λ); namely n can vary from 2.43 for $\lambda < 300$ nm to $n < 1$ for $\lambda > 600$ nm.[18] In this respect, TiN appears to be an ideal candidate for serving as the coating layer for exploring the optical and electrical properties of Si-NSs.

In this study, we further introduce a lithography-free self-masking method to fabricate a wafer-scale Si nano-pillar (Si-NP) array. This process involves only a single-step hydrogen plasma dry etching directly applied to a wafer-size silicon substrate

[a]*Department of Electrophysics, National Chiao Tung University, Hsinchu 300, Taiwan. E-mail: ymchang7@gmail.com; jyjuang@g2.nctu.edu.tw; Fax: +886-3-5725230; Tel: +886-3-5712121 ext. 56116*

[b]*Department of Materials Science and Engineering, National Chiao Tung University, Hsinchu 300, Taiwan*

[c]*Center for Measurement Standards, Industrial Technology Research Institute, Hsinchu 300, Taiwan*

[d]*Department of Materials Science and Engineering, National United University, Miaoli 360, Taiwan*

This journal is © The Royal Society of Chemistry 2014

Published on 17 June 2014. Downloaded by National Chiao Tung University on 25/12/2014 02:11:40.

without introducing any metal nano-dots or other etching masks. As a result, it represents an extremely simple and effective way of fabricating large area Si-NSs. The as-made Si-NPs exhibit an average reflectance of 1.79% over the wavelength range of 380–1000 nm. Although it is by far superior to that obtained in most antireflective Si-NSs, an undesired uprising in reflectivity for wavelengths beyond 1000 nm was observed. Nevertheless, by depositing a thin layer of TiN, not only the long-wavelength (>1 μm) reflectivity is drastically improved but also the corresponding field emission properties of the Si-NPs are significantly enhanced. The effects of the TiN layer thickness are discussed with the aid of detailed microstructural analyses to delineate the underlying mechanisms relevant to the obtained results.

Experimental section

The wafer-scale production of Si-NPs was carried out in an inductively coupled plasma chemical vapor deposition (ICPCVD) system using the following processes. Prior to performing the etching processes, CF_4 and O_2 plasma were applied to clean the chamber. After the Si(100) wafer was loaded into the reactive chamber, it was pumped to a pressure of 5×10^{-5} Torr with the substrate holder being heated to 400 °C. Subsequently, the H_2 gas with a flow rate of 160 sccm was introduced into the reactor with the pressure maintained at 30 mTorr. The etching process was carried out by maintaining the input radio-frequency (RF) and dc-bias power at 550 W and 280 W, respectively. Details of the process parameters and the possible mechanisms involved in obtaining Si-NPs with H_2-plasma etching were described and discussed previously.[19–23] However, unlike that practiced previously, in this study the duration of H_2-plasma etching has been increased to 120 min. Ultrathin TiN films were deposited onto these nanopillar covered Si substrates at an ambient temperature of 470 °C by atomic layer deposition (ALD). ALD growth is a self-limiting vapor-phase chemisorption process governed primarily by consecutive surface reactions. Thus, in order to precisely control each surface reaction step, critical purge steps were usually conducted to prevent individual reactive precursors from mutual interactions.[24] In the present study, pulse durations of ammonia and titanium chloride ($TiCl_4$) precursors were both kept at 0.5 seconds and the purge and pumping periods were maintained at 10 seconds. Argon (Ar) gas was used as the purge gas with the pressure being set to 0.8 Torr. The above deposition scheme was used for depositing ultrathin TiN films onto the surface of Si-NPs for 90, 180, 360 and 540 ALD cycles, which resulted in the corresponding TiN film thickness of about 5, 10, 15 and 20 nm, respectively.

A field emission scanning electron microscope (FESEM, JEOL JSM-6700F) was used to examine the morphology of the TiN/Si-NP heterostructures. High-resolution X-ray diffraction (HRXRD, PANalytical X'Pert Pro Singapore, with Cu Kα; $\lambda = 0.154$ nm) was used to determine the phase formation and crystallographic structure of all samples. High resolution transmission electron microscopy (HRTEM, JEOL JEM-2010F) with an operating voltage of 200 kV was employed to investigate the interface microstructures of the obtained TiN/Si-NP heterostructures. The reflectivity of the bare Si-NPs and TiN/Si-NPs was measured using a spectrophotometer (Jasco V-670) with unpolarized light of wavelength ranging from 380 to 1500 nm. In order to obtain precise information on the optical properties of the Si-NPs and TiN/Si-NPs, an integrating sphere was used in the spectrophotometer to determine the total reflectance.[25] Moreover, the samples were loaded into a vacuum chamber (2×10^{-6} Torr) to measure the field emission current. The probe served as the anode electrode in the vacuum system and the cathode voltage was applied to the Si substrates.

Results and discussion

The FESEM image shown in Fig. 1a displays the typical morphology of the Si-NPs obtained by the present single-step plasma etching process. As is evident from the image, the Si-NPs are about 300–600 nm in height and are aligned vertically with an average diameter of about 40–60 nm and a density of $\sim 3 \times 10^{12}$ cm^{-2}. Fig. 1b shows the top-view SEM image of the Si-NPs, indicating that the individual nano-pillars are indeed well-separated with an average spacing of ∼50–60 nm. Furthermore, as shown in Fig. 1c, the HRTEM image shows that the obtained Si-NPs remain essentially single crystalline, indicating that the present single-step plasma etching process apparently has resulted in effective anisotropic vertical etching while only leading to negligible damage laterally, a characteristic feature of dc-biased low-pressure reactive plasma etching.[19] In addition, the optical micrograph displayed in Fig. 1d exhibits that the appearance of the entire 6-inch wafer becomes dark black, presumably due to the enhanced antireflectivity resulting from the layer of the obtained densely packed array of Si-NPs.

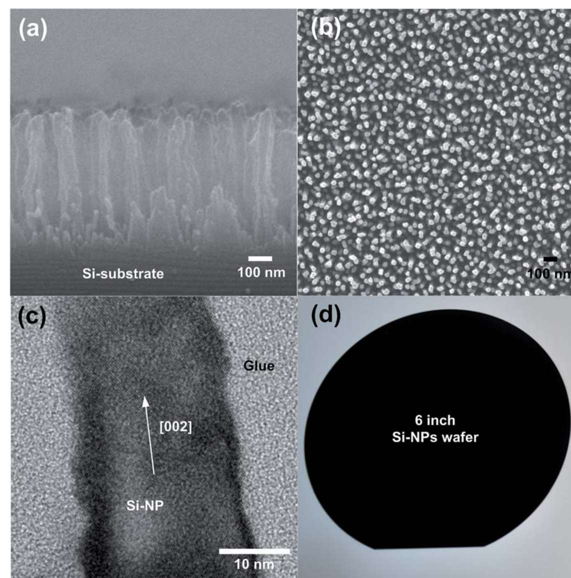

Fig. 1 (a) Cross-sectional and (b) top-view SEM images of Si-NPs. (c) The HRTEM image of Si-NPs, and (d) the Si-NP-coated wafer exhibited a uniformly dark surface, *i.e.*, excellent light trapping properties over the entire surface of the 6 inch Si wafer.

Published on 17 June 2014. Downloaded by National Chiao Tung University on 25/12/2014 02:11:40.

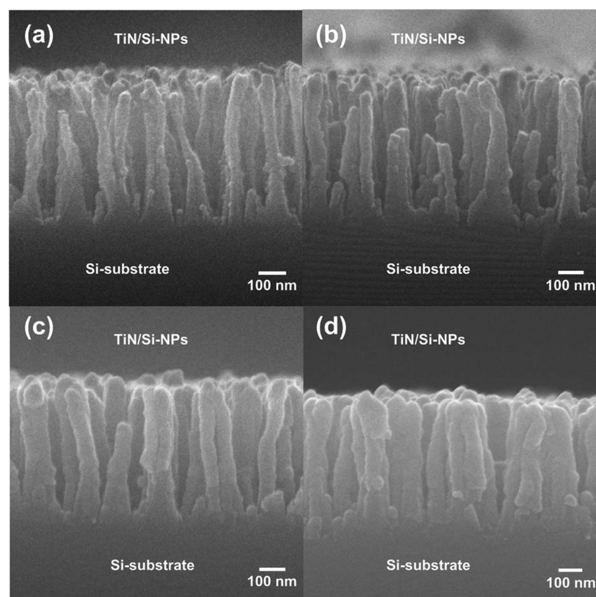

Fig. 2 Cross-sectional SEM images of a (a) 5 nm, (b) 10 nm, (c) 15 nm and (d) 20 nm TiN film which was grown on Si-NPs.

Fig. 2 shows the typical cross-sectional image of the TiN-coated Si-NPs. The thicknesses of the ALD grown TiN layer are 5, 10, 15, and 20 nm as shown in Fig. 2a–d, respectively. It is clear that, when compared with the as-prepared Si-NPs displayed in Fig. 1a and b, the morphology of the vertically aligned Si-NPs remains essentially intact after depositing a layer of 5 or 10 nm thick TiN films. However, the pillars appear to coalesce (Fig. 2c and d) as the thickness of the TiN layer is further increased. The effects of this morphological change on the antireflectivity and field emission properties of the TiN/Si-NPs will be examined in more detail below.

In order to examine the structure of the thin TiN layers deposited on the Si-NP array, the grazing incidence XRD measurements were carried out. Fig. 3 shows the XRD patterns obtained for the TiN films with various thicknesses (5, 10, 15 and 20 nm, respectively) on Si-NPs. It is evident that all samples exhibit the formation of the polycrystalline TiN phase. Furthermore, the grain size of the TiN films appears to increase with the increasing film thickness as indicated by the decreasing full-width at half-maximum (FWHM) of the corresponding diffraction peaks. A rough estimate on the grain size using the Scherrer's formula:[26,27] $D = K\lambda/\beta \cos \theta$, where D is the grain size, K ($\sim$0.9) is a constant, λ is the wavelength, β and θ are the FWHM and angle of the chosen diffraction peak, respectively, indicates that the grain size is about 5, 6, 8, and 10 nm for a TiN thickness of 5, 10, 15 and 20 nm, respectively.

To further confirm the structural information suggested by the XRD results for the obtained TiN films in more detail, we examined the TiN/Si-NP heterostructures by HRTEM. The HRTEM image, as shown in Fig. 4, evidently reveals that the interface of TiN/Si-NP heterostructures is nearly free of an oxide layer. Moreover, it can be seen that the 10 nm thick TiN layer is indeed of polycrystalline nature with an average grain size of 6–7 nm, which is in good agreement with the XRD results shown in Fig. 3. In any case, we have demonstrated that the TiN layer with varying thicknesses can be uniformly coated onto the Si-NPs fabricated by self-masking dry etching in hydrogen-containing plasma.

Next we discuss the optical and electronic properties of the obtained TiN/Si-NP heterostructures. The total reflectance spectra, including the specularly reflected beam, over the wavelength range of 380–1500 nm were recorded in an integrating sphere. For comparison the total reflectance of the polished Si substrate is included. As is evident from the results shown in Fig. 5, the polished Si substrate exhibits a monotonically decreasing reflectance with an average of $\sim$33.6% in the wavelength range of 380–1000 nm, and then displays an abrupt up-rise to about 45% for the wavelength beyond 1000 nm. The reflectance is significantly suppressed to an average of 1.49% in the range of 380–1000 nm when the surface is covered by a layer of as-fabricated Si-NPs. The more than one

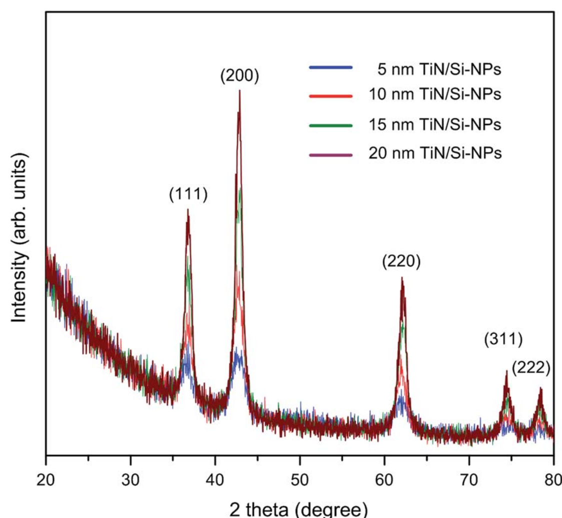

Fig. 3 XRD curves of 5 nm TiN/Si-NPs (blue line), 10 nm TiN/Si-NPs (red line), 15 nm TiN/Si-NPs (green line), and 20 nm TiN/Si-NPs (wine line).

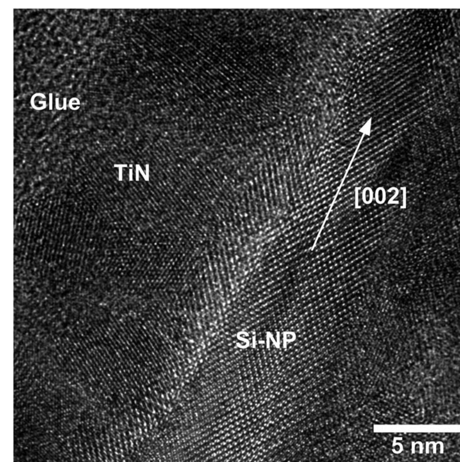

Fig. 4 Image of HRTEM for the 10 nm TiN/Si-NP heterostructure.

This journal is © The Royal Society of Chemistry 2014

Published on 17 June 2014. Downloaded by National Chiao Tung University on 25/12/2014 02:11:40.

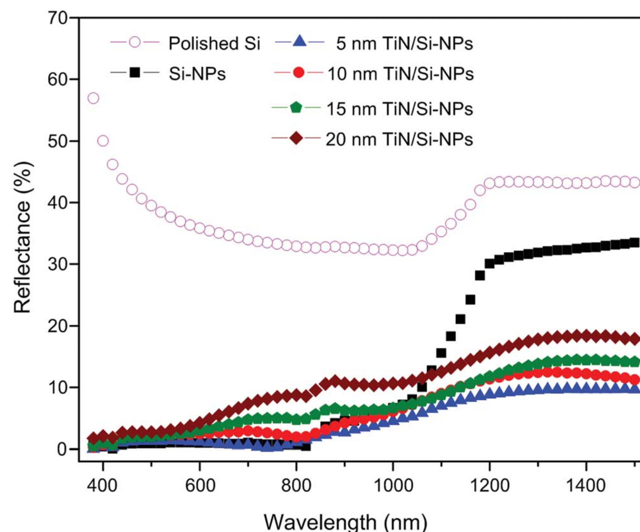

Fig. 5 The reflectance curves of polished Si (empty circles) and bare Si-NPs (black squares), 5 nm TiN/Si-NPs (solid triangles), 10 nm TiN/Si-NPs (solid circles), 15 nm TiN/Si-NPs (solid pentagon), and 20 nm TiN/Si-NPs (solid diamond).

order of magnitude improvement in reflectance is attributed to the reduction of the effective refraction index in the Si-NP layer by introducing more empty space, as well as the greatly increased surface area and formation of a gradually decreasing refraction index gradient from the substrate to air because of the tapered pillars.[6–8,20] The reflectance of the as-fabricated Si-NPs, however, increases abruptly for the illuminating wavelength beyond 1100 nm. This phenomenon is similar to that seen in the polished Si substrate and may be attributed to the fact that the photon energy is already smaller than the energy gap of Si (~1.1 eV at room temperature)[28] and the light is hardly absorbed by the Si-NP-coated substrate. Alternatively, since the illuminating wavelength has become larger than the height of the nano-pillars, the destructive interference from the nano-pillars becomes less effective, leading to an abrupt increase in reflectance.[19]

Perhaps the most interesting observation of the present study is wavelength dependent reflectance exhibited by the TiN-coated Si-NPs. As can be seen from Fig. 5, while the short wavelength reflectance (from 380 to 1000 nm) of TiN/Si-NPs is slightly increased with increasing thickness of the TiN layer, the long wavelength reflectance in these TiN/Si-NPs is, nevertheless, displaying a very different behavior as compared to that of the polished Si substrate and as-fabricated Si-NPs. As is suggestive from the morphological evolution of TiN coating, the slight increase of reflectance with the increasing thickness of the TiN layer in the short wavelength range might be explained by blunting of Si-NP tips and the coalescence of neighboring Si-NPs (Fig. 2a–d). The tips of the nano-pillars get larger in diameter and become less conducive to optical coupling. Moreover, the TiN coating also fills more and more empty spaces existing in the original Si-NPs, leading to a slight increase in the effective refractive index as well as to the blurring of the tapering structure. The manifestation of the abovementioned two factors, namely the diameter of the nano-pillar's tip and the inter-pillar spacing, has indeed resulted in a sizeable increase in reflectivity for TiN/Si-NPs below a wavelength of 800 nm, except for the 5 nm one. The slight decrease of reflectance for the 5 nm TiN/Si-NPs may thus be explained by being due to the competition between the optical coupling effect of nano-pillar's tip and reduced reflectivity induced by inter-pillar spacing modifications. Nevertheless, compared to the as-fabricated Si-NPs, the reflectance of all TiN/Si-NP heterostructures is significantly reduced in the wavelength range beyond 1000 nm. In general, effective antireflective coating relies primarily on the following factors: (i) $n_c \sim (n_a n_s)^{1/2}$, where n_c, n_a, and n_s are refractive indices of the coating material, air, and substrate, respectively; (ii) the layer thickness near the quarter-wavelength optical thickness; (iii) establishment of some sort of refractive index gradient.[8] Since the Si-NPs fabricated by the present one-step process are rather uneven, making it rather difficult to quantitatively estimate the relative volume ratio between the empty inter-pillar spaces and pillars with or without TiN coatings, hence a meaningful effective refractive index gradient. Nevertheless, it is natural to expect that the refractive index gradient is modified (in fact, deteriorated) with increasing thickness of the TiN coating layer owing to decreasing empty inter-pillar spacing. This, in fact, is reflected in the results seen in the short wavelength region, where the reflectance is increased with increasing thickness of the TiN layers. Thus, the improvement of antireflection characteristics in the long wavelength range obtained here is more likely due to the dramatic reduction of the refractive index of the TiN layer in the long wavelength range (from $n \sim 2.43$ at $\lambda < 230$ nm to $n \sim 0.98$ at $\lambda > 900$ nm),[18] instead of refractive index gradient modifications in the present case. This observation also suggests that, by carefully manipulating the morphology and the inter-pillar spacing, further improvement on the broadband antireflection can be achieved. The next question of interest will be how the coated TiN thin layer affects the electronic properties of the Si-NPs and the associated field emission performance for these nanopillar structures. Fig. 6 shows the emission current density as a function of the applied electrical field (*J*–*E* curves) for both the Si-NPs and TiN/Si-NPs. The electric field was determined by dividing the applied voltage with the apparent cathode–anode separation. Thus, it represents an averaged global field instead of a local field at the tips of the nanostructures. Steady field emission was obtained by keeping the distance between the electrodes at 25–45 μm and the chamber pressure at 2×10^{-6} Torr during measurements. It is evident from Fig. 6 that, for the as-fabricated Si-NPs, only a diminishingly small field emission current was detected up to the maximum applied field (~44 V μm^{-1}) of the current setup. Moreover, the turn-on field, which was defined as the applied field required for drawing an emission current of 200 μA cm^{-2}, is 30.2 V μm^{-1}. This is presumably due to the existence of the native oxide layer which forms an insurmountable barrier for electron emission. On the other hand, for the TiN(10 nm)/Si-NPs, the turn-on field is significantly reduced to ~13.3 V μm^{-1}. It is noted that the emission current density reaches ~4 mA cm^{-2} at the maximum bias field of our current setup

Published on 17 June 2014. Downloaded by National Chiao Tung University on 25/12/2014 02:11:40.

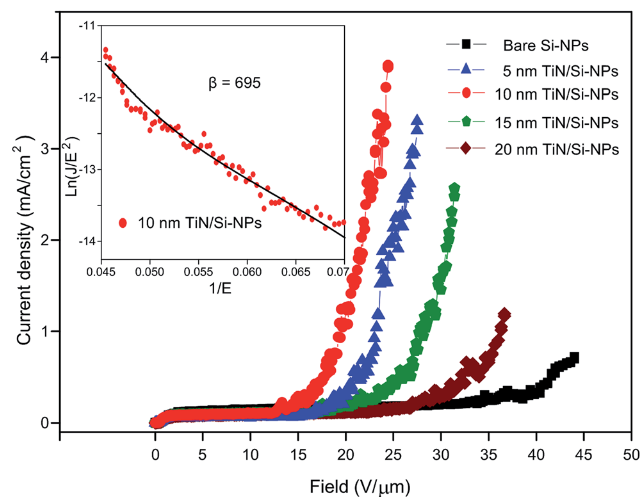

Fig. 6 Field-emission characteristics of bare Si-NPs (squares), 5 nm TiN/Si-NPs (triangles), 10 nm TiN/Si-NPs (circles), 15 nm TiN/Si-NPs (pentagon), and 20 nm TiN/Si-NPs (diamond). The inset shows the F–N plot of the corresponding field-emission data for 10 nm TiN/Si-NPs.

(24.4 V μm^{-1}). We believe that the enhancement of field emission for all TiN/Si-NPs obtained in this study was resulted from the combination with the geometric morphology of Si-NPs as well as the interface and electronic structure modifications arising from the coated transparent conductive TiN layer. In particular, as is evident from Fig. 4b, TiN-coating appears to have removed the formation of the native SiO_x layer completely from the surface of Si-NPs, which might account for the substantial reduction of the field emission threshold voltage.

According to the classical Fowler–Nordheim (F–N) theory for field emission the relationship between the emission current density and the applied field can be expressed by the following F–N equation:[29–34]

$$J = \frac{A\beta^2 E^2}{\phi} \exp\left(\frac{-B\phi^{3/2}}{\beta E}\right) \quad (1)$$

where J is the current density (A m^{-2}), E is the applied field (V μm^{-1}), ϕ is the work function (eV), β is the field enhancement factor, A and B are constants with $A = 1.56 \times 10^{-10}$ (A eV V^{-2}) and $B = 6.83 \times 10^3$ (V μm^{-1} eV$^{-3/2}$), respectively. From eqn (1), it is clear that the two primary parameters determining the emission characteristics of a particular structure are ϕ and β, which can be obtained experimentally by plotting $\ln(J/E^2)$ *vs.* $1/E$, the so-called F–N plot. The inset in Fig. 6 shows the F–N plot of the corresponding field emission data of the TiN(10 nm)/Si-NPs, which evidently exhibits a nearly straight line. The quasi-linear behavior of the plot indicates that the field emission behavior of these heterostructures may have deviated from the F–N description slightly. It should be noted that the original F–N theory was derived specifically for flat, metallic surfaces with work function on the order of 2–5 eV.[32] Thus, it might not be as exact when applied to other materials or to structures with different morphologies. It is, nevertheless, still an instructive practice to make some quantitative estimates using the F–N theory. The field enhancement factor β was calculated from the slope of the F–N plot as $\beta = -6.83 \times 10^3 \times \phi^{3/2}$/slope. By assuming the work function of $\phi = 4.7$ eV for TiN,[13] a β value of 695 was obtained (inset in Fig. 6). The value is somewhat smaller than those obtained from ZnO- and Au-coated Si-NPs,[9,33] presumably due to the blunting and densely packed morphology of the present one-step plasma etched Si-NPs. However, the fact is that, by starting with the same Si-NPs, significant enhancement in field emission properties indeed can be obtained by TiN-coating. Thus, we believe that suitable combination of the morphological feature and surface modification could result in excellent field emission characteristics in a controllable manner.

Conclusion

In summary, we have demonstrated the viability of a self-masking hydrogen-containing dry etching scheme in fabricating well-aligned Si-NPs directly on the Si substrate. The as-fabricated Si-NPs exhibit drastic reduction in antireflectance over the wavelength range of 380–1000 nm due to sub-wavelength scattering and reduced refractive index gradient. However, similar to the as-polished Si substrate, the reflectance of the structure displayed a sudden increase in the longer wavelength region. By introducing a layer of TiN-coating on the Si-NPs, substantial improvement of antireflectance in the long wavelength range is observed, which is believed to result from the drastic change in the refractive index of TiN when the wavelength exceeds 600 nm. The coating of TiN also results in suppression of SiO_x formation at the surface of Si-NPs and modification of the effective work function of the TiN/Si-NP heterostructures, leading to significant improvement in field emission properties. The present study thus indicates an efficient and effective scheme for obtaining 1D-Si nanostructures with outstanding perspectives in opto-electrical applications.

Acknowledgements

This work was partially supported by the National Science Council of Taiwan, under Grant no.: NSC102-2811-M-009-052. Prof. J.-Y. Juang is supported in part by the National Science Council of Taiwan and the MOE-ATU program operated at NCTU. The authors would like to thank Dr Yu-Hwa Shih, Prof. Chih-Ming Lin (NHUE), Dr Hsin-Yi Lee (NSRRC and NCTU), Dr Jheng-Ming Huang (NCTU), Dr Shang-Jui Chiu (NTHU) and Dr Yen-Ting Liu (NCTU) for useful discussion and Dr Chun-Wei Huang (NCTU) for TEM.

Notes and references

1 Y. Qu, H. Zhou and X. Duan, *Nanoscale*, 2011, **3**, 4060.
2 T.-H. Chang, K. Panda, B. K. Panigrahi, S.-C. Lou, C. Chen, H.-C. Chan, I.-N. Lin and N.-H. Tai, *J. Phys. Chem. C*, 2012, **116**, 19867.
3 F.-Y. Wang, Q.-D. Yang, G. Xu, N.-Y. Lei, Y. K. Tsang, N.-B. Wong and J. C. Ho, *Nanoscale*, 2011, **3**, 3269.
4 J. B. Hannon, S. Kodambaka, F. M. Ross and R. M. Tromp, *Nature*, 2006, **440**, 69.

This journal is © The Royal Society of Chemistry 2014

Published on 17 June 2014. Downloaded by National Chiao Tung University on 25/12/2014 02:11:40.

5 S. W. Boettcher, J. M. Spurgeon, M. C. Putnam, E. L. Warren, D. B. Turner-Evans, M. D. Kelzenberg, J. R. Maiolo, H. A. Atwater and N. S. Lewis, *Science*, 2010, **327**, 185.
6 S.-C. Tseng, H.-L. Chen, C.-C. Yu, Y.-S. Lai and H.-W. Liu, *Energy Environ. Sci.*, 2011, **4**, 5020.
7 G.-R. Lin, Y.-C. Chang, E.-S. Liu, H.-C. Kuo and H.-S. Lin, *Appl. Phys. Lett.*, 2007, **90**, 181923.
8 Y.-M. Chang, J. Shieh and J.-Y. Juang, *J. Phys. Chem. C*, 2011, **115**, 8983.
9 Y.-M. Chang, M.-C. Liu, P.-H. Kao, C.-M. Lin, H.-Y. Lee and J.-Y. Juang, *ACS Appl. Mater. Interfaces*, 2012, **4**, 1411.
10 J. P. Thomas, H.-C. Chen, S.-H. Tseng, H.-C. Wu, C.-Y. Lee, H. F. Cheng, N.-H. Tai and I.-N. Lin, *ACS Appl. Mater. Interfaces*, 2012, **4**, 5103.
11 J. Liu, V. V. Zhirnov, G. J. Wojak, A. F. Myers, W. B. Choi, J. J. Hren, S. D. Wolter, M. T. McClure, B. R. Stoner and J. T. Glass, *Appl. Phys. Lett.*, 1994, **65**, 2842.
12 H. O. Pierson, *Handbook of refractory carbides and nitrides: properties, characteristics, processing, and applications*, William Andrew, 1996, p. 193.
13 L. R. C. Fonseca and A. A. Knizhnik, *Phys. Rev. B: Condens. Matter Mater. Phys.*, 2006, **74**, 195304.
14 Y. Liu, S. Kijima, E. Sigimata, M. Masahara, K. Endo, T. Matsukawa, K. Ishii, K. Sakamoto, T. Sekigawa, H. Yamauchi, Y. Takanashi and E. Suzuki, *IEEE Trans. Nanotechnol.*, 2006, **5**, 723.
15 M. Kadoshima, T. Matsuki, S. Miyazaki, K. Shiraishi, T. Chikyo, K. Yamada, T. Aoyama, Y. Nara and Y. Ohij, *IEEE Electron Device Lett.*, 2009, **30**, 466.
16 A. Didden, H. Battjes, R. Machunze, B. Dam and R. van de Krol, *J. Appl. Phys.*, 2011, **110**, 033717.
17 F. Fillot, T. Morel, S. Minoret, I. Matko, S. Maîtrejean, B. Guillaumot, B. Chenevier and T. Billon, *Microelectron. Eng.*, 2005, **82**, 248.
18 Y. Claesson, M. Georgson, A. Roos and C.-G. Ribbing, *Sol. Energy Mater.*, 1990, **20**, 455.
19 J. Shieh, C. H. Lin and M. C. Yang, *J. Phys. D: Appl. Phys.*, 2007, **40**, 2242–2246.
20 Y.-M. Chang, J. Shieh, P.-Y. Chu, H.-Y. Lee, C.-M. Lin and J.-Y. Juang, *ACS Appl. Mater. Interfaces*, 2011, **3**, 4415.
21 J. Shieh, F. J. Hou, Y. C. Chen, H. M. Chen, S. P. Yang, C. C. Cheng and H. L. Chen, *Adv. Mater.*, 2010, **22**, 597.
22 J. Shieh, S. Ravipati, F.-H. Ko and K. Ostrikov, *J. Phys. D: Appl. Phys.*, 2011, **44**, 174010.
23 Y.-M. Chang, S.-R. Jian, H.-Y. Lee, C.-M. Lin and J.-Y. Juang, *Nanotechnology*, 2010, **21**, 385705.
24 H. Tiznado and F. Zaera, *J. Phys. Chem. B*, 2006, **110**, 13491.
25 Y.-M. Chang, C.-L. Dai, T.-C. Cheng and C.-W. Hsu, *Thin Solid Films*, 2010, **518**, 3782.
26 A. L. Patterson, *Phys. Rev.*, 1939, **56**, 978.
27 Y.-M. Chang, C.-L. Dai, T.-C. Cheng and C.-W. Hsu, *Appl. Surf. Sci.*, 2008, **254**, 3105.
28 V. Alex, S. Finkbeiner and J. Weber, *J. Appl. Phys.*, 1996, **79**, 6943.
29 Y. Li, X. Fang, N. Koshizaki, T. Sasaki, L. Li, S. Gao, Y. Shimizu, Y. Bando and D. Golberg, *Adv. Funct. Mater.*, 2009, **19**, 2467.
30 Y.-M. Chang, M.-L. Lin, T.-Y. Lai, H.-Y. Lee, C.-M. Lin, Y.-C. Wu and J.-Y. Juang, *ACS Appl. Mater. Interfaces*, 2012, **4**, 6676.
31 Y.-M. Chang, J.-M. Huang, C.-M. Lin, H.-Y. Lee, S.-Y. Chen and J.-Y. Juang, *J. Phys. Chem. C*, 2012, **116**, 8332.
32 R. Schlesser, M. T. McClure, B. L. McCarson and Z. Sitar, *J. Appl. Phys.*, 1997, **82**, 5763.
33 Y.-M. Chang, P.-H. Kao, H.-W. Wang, H.-M. Tai, C.-M. Lin, H.-Y. Lee and J.-Y. Juang, *Phys. Chem. Chem. Phys.*, 2013, **15**, 10761.
34 Y.-M. Chang, P.-H. Kao, M.-C. Liu, C.-M. Lin, H.-Y. Lee and J.-Y. Juang, *RSC Adv.*, 2012, **2**, 11089.

This journal is © The Royal Society of Chemistry 2014